Formation of solid SiO_2He compound at high pressure and high temperature

Shicong Ding,[1] Pan Zhang,[1] Kang Yang,[1] Cailong Liu,[2] Jian Hao,[1] Wenwen Cui,[1,*] Jingming Shi,[1,†] and Yinwei Li[1,2,‡]

[1]*Laboratory of Quantum Functional Materials Design and Application, School of Physics and Electronic Engineering, Jiangsu Normal University, Xuzhou 221116, China*

[2]*Shandong Key Laboratory of Optical Communication Science and Technology, School of Physical Science & Information Technology, Liaocheng University, Liaocheng 252059, China*

(Received 2 July 2021; revised 6 June 2022; accepted 28 June 2022; published 6 July 2022)

Silica, a main mineral inside the Earth and super-Earth, is generally assumed to be resistant to react with noble gas elements at ambient conditions. Here, combining crystal structural prediction and first-principles calculation, we predict a SiO_2He compound that becomes stable at high pressure. Each Si (He) atom in the SiO_2He is bonded with seven O atoms and two He (Si) atoms, forming a Si-centered SiO_7He_2 (He-centered HeO_7Si_2) polyhedron. Further calculations indicate that the SiO_2He compound remains solid over a wide range of pressures exceeding 607 GPa and temperatures of 0–9000 K, covering the extreme conditions of the core-mantle boundary in super-Earth exoplanets or even in the ice giants of our solar system. Our results may provide theoretical guidance for the discovery of other silicides at high pressures, which promote the exploration of materials at planetary core-mantle boundaries, and enable planetary models to be refined as well.

DOI: 10.1103/PhysRevB.106.024102

I. INTRODUCTION

Silica (SiO_2) is the main component of silicates in the core-mantle boundary (CMB) of the Earth and super-Earth exoplanets (1–10 times Earth's mass, $M_\oplus$). Elucidating the variation of Si's coordination number (CN) in SiO_2 has therefore attracted much recent attention in the field of planetary science [1–3]. At ambient conditions, SiO_2 adopts the quartz structure with four-coordinated Si [4]. This structure transforms into a coesite phase, at ∼2 GPa [5], and then successively transforms to four six-coordinated high-pressure phases: a stishovite phase at ∼10 GPa [6,7], a $CaCl_2$-type structure at ∼48 GPa [8], a α-PbO_2-type structure at ∼82 GPa [9,10], and a pyrite-type structure at ∼260 GPa [11,12]. Previous studies have observed a continuously increasing CN of Si from 6.0 to 6.8 with increasing pressure in amorphous SiO_2 [13,14], while recent theoretical studies have proposed several candidate structures for SiO_2 with a higher CN for Si at higher pressures: a $R\bar{3}$ structure with mixed six-, eight-, and nine-coordinated Si that becomes stable at 645 GPa [15], a nine-coordinated Fe_2P-type structure at 890 GPa [2,15], and a ten-coordinated $I4/mmm$ phase at 10 TPa [16]. Experimental and theoretical studies have also determined a metastable coesite-IV phase at 30–50 GPa that contains five-coordinated Si [17]. Generally, the greater the depth in a planet, the higher the pressure and greater the density. An increase in density is generally accompanied by an increase in CN, with a linear increase in density possibly being associated with a linear increase in CN. Therefore, the investigation on the variety of CN in silica at high pressure has significant influence not only in condensed matter physics but also the geoscience.

Planetary interiors are naturally extremely hot, pressurized, and rich in silica. Understanding the silica structure before it has melted under extreme conditions is the key to determining a planet's internal structure and evolution. In 2015, Millot *et al.*'s laser-driven shock experiment found that the melting temperature of silica rises to 8300 K at a pressure of 500 GPa, comparable to the CMB of a super-Earth of 5 $M_\oplus$ [3]. However, laboratory experiments face several challenges when reproducing the conditions of giant planets or super-Earths [18]. Theoretical modeling can effectively simulate extreme conditions and so aids in the exploration of the behavior of minerals such as SiO_2 inside planets [2,19–22]. Using first-principles molecular dynamics simulations, Scipioni *et al.* found that under conditions of the early Earth's and super-Earths' deep molten mantles, the electron conductivity of liquid SiO_2 is sufficiently large to support a silicate dynamo [19]. González-Cataldo *et al.* studied the melting curves of SiO_2 up to 6 TPa using first-principles molecular dynamics simulations, finding that SiO_2 is solid under the conditions of the cores of all the solar system's gas giants and also super-Earths of 10 $M_\oplus$ [20]. Tsuchiya *et al.* and Wu *et al.* independently proposed that the cores of Uranus and Neptune are expected to consist of Fe_2P-type silica and $MgSiO_3$ [2,22]. Niu *et al.*'s structural prediction of the Mg-Si-O ternary phase diagram under exoplanet pressure revealed two novel compounds, Mg_2SiO_4 and $MgSi_2O_5$, as being stable at the CMB of large super-Earths [21]. Overall, these studies make important contributions to the understanding of the physicochemical diversity of planetary systems.

Helium is the second most abundant element in the universe, and is extensively present in stars and gas giant planets [23,24]. It is usually chemically inert and does not react

*wenwencui@jsnu.edu.cn
†jingmingshi@jsnu.edu.cn
‡yinwei_li@jsnu.edu.cn

easily with other substances at ambient conditions due to its closed-shell electronic configuration. The melting and volcanic effects of the early Earth's mantle caused He in the upper mantle to escape via internal degassing and disappear into space, while a layer of the lower mantle continues to retain He [25]. Recent studies have shown that FeO_2 can react with He near the Earth's CMB to trap He in the lower mantle [26,27]. Ice giants are mainly composed of H_2O, NH_3, and CH_4; their atmospheres are rich in He [23,28]. Theoretical studies have shown that H_2O [29–31], NH_3 [31–33], and CH_4 [34] can form stable compounds with He at high pressure, and first-principles molecular dynamics suggests that both H_2O-He and NH_3-He may exist in a superionic state in the interiors of icy planets, in addition to the plastic state of NH_3-He and the plastic or partially diffusive state of CH_4-He at lower pressures and temperatures. Theoretical work has reported that He can form stable crystalline compounds with iron at terapascal pressures [35]. Other recent studies have reported the high-pressure stability of He-alkali oxides (sulfides) [36], HeN_4 [37], Na_2He [38], $Mg(Ca)F_2He$ [39], $XeHe_2$ [40], and Si_2He [41]. In addition, previous studies have shown that the insertion of He into cristobalite can greatly decrease its compressibility, resulting in two cristobalite-helium compound phases, i.e., I ($P2_1/c$, stable above 6.4 GPa) and II ($R\bar{3}c$, at 1.7–6.4 GPa) [42,43]. Therefore, He is the candidate worth studying for mixing with SiO_2 to investigate the CN of silicon, the potential mineral, and the resulting material at high pressure.

Combining density functional theory and structural prediction, this paper presents an extensive exploration of the SiO_2-He system at high pressure and high temperature. The results show that He can react with SiO_2 to form SiO_2He at high pressures, and first-principles molecular dynamics simulations indicate that the SiO_2He retains its solid character at high temperatures. Both Si and He atoms in SiO_2He have a coordination number of nine: Each Si atom is bonded with seven O atoms and two He atoms, while each He atom is bonded with seven O atoms and two Si atoms, forming Si-centered SiO_7He_2 or He-centered HeO_7Si_2 polyhedra, respectively. These results may provide theoretical guidance for the discovery of other silicides at high pressures.

II. COMPUTATIONAL METHODS

Structure predictions for the SiO_2-He system are performed here using CALYPSO [44–46], based on a global minimization of free-energy surfaces in conjunction with *ab initio* total energy calculations, which has been used successfully to predict various systems [47,48], especially on superconductors [49–54] and planetary minerals [32,55,56] under high pressure. Structural relaxations are performed using density functional theory as implemented in the Vienna *ab initio* simulation package [57,58], adopting the Perdew-Burke-Ernzerhof exchange-correlation functional under the generalized gradient approximation [59,60]. All-electron projector augmented-wave pseudopotentials with $3s^23p^2$, $2s^22p^4$, and $1s^2$ valence configurations are chosen for Si, O, and He atoms, respectively [61]. Structure searches use a plane-wave cutoff energy of 1000 eV and a k-point mesh of $2\pi \times 0.04$ Å^{-1}. The lowest-energy structural optimization and electronic

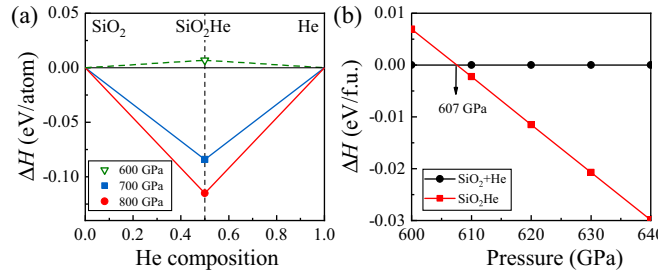

FIG. 1. (a) Convex hull for formation enthalpies (ΔH) of the SiO_2-He system at selected pressures, defined as $\Delta H = \{H[(SiO_2)_xHe_y] - xH(SiO_2) - yH(He)\}/(3x + y)$. (b) Calculated formation enthalpy of SiO_2He relative to decomposition products SiO_2 (pyrite type at 600 GPa, $R\bar{3}$ at 700 and 800 GPa) and He (hcp at 600–800 GPa) as a function of pressure.

properties are calculated using "hard" pseudopotentials with $2s^22p^63s^23p^2$ and $2s^22p^4$ valence configurations for Si and O atoms, respectively. A plane-wave cutoff energy of 1500 eV and k-point mesh of $2\pi \times 0.03$ Å^{-1} are set to ensure total energy and force convergence better than 1 meV/atom and 1 meV/Å, respectively. Phonon calculations are carried out using a supercell approach, as implemented in the PHONOPY code [62]. *Ab initio* molecular dynamics (AIMD) simulations [63] explore the form of SiO_2He compounds at high pressures and high temperatures, adopting the NVT (N is the number of particles, V the volume, and T temperature) ensemble by using a Nosé-Hoover thermostat [64] with SMASS = 2. A $2 \times 3 \times 3$ supercell of 288 atoms is employed, along with Γ point sampling of the Brillouin zone. The crystal structures and electron localization function (ELF) are plotted using VESTA software [65].

III. RESULTS AND DISCUSSION

Extensive structure searches for $(SiO_2)_xHe_y$ (x, y = 1-3) are performed at 100–800 GPa with maximum simulation cells up to four formula units (f.u.) at each composition. Figure 1(a) summarizes the formation enthalpies (ΔH) of the stoichiometries with respect to decomposition into SiO_2 and He, with positive formation enthalpies above 0.05 eV/atom not shown in the convex hull. The stoichiometry of SiO_2He has a negative formation enthalpy at 700 and 800 GPa, whose ΔH approaches zero at ~607 GPa, as shown in Fig. 1(b). This reveals that the SiO_2He compound is thermodynamically stable when the pressure is above this critical pressure.

The predicted SiO_2He phase has an orthorhombic structure with space group *Pnma* (4 f.u. in a unit cell) and remains stable up to 1000 GPa, the maximum pressure studied here. Figure 2(a) shows its structural configuration, and Table S1 in the Supplemental Material (SM) summarizes the detailed structural parameters [66]. Further analysis of the atomic positions shows that the Si atoms are surrounded by seven O atoms and two He atoms with the Si-O distances ranging from 1.54 to 1.67 Å and a Si-He distance of 1.57 Å at 610 GPa, leading to the formation of four unexpected SiO_7He_2 polyhedra in its unit cell. Two SiO_7He_2 polyhedra in the center of the cell connect with each other by sharing edges, and link the top and bottom polyhedra by sharing one O atom.

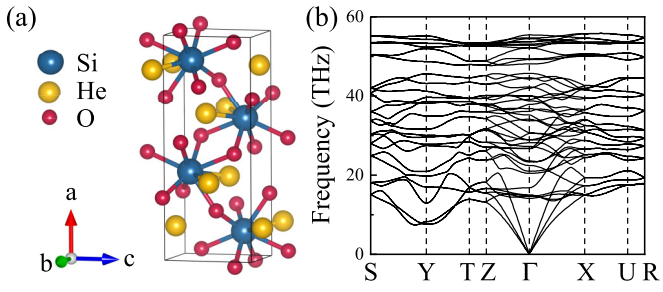

FIG. 2. (a) Crystal structure predicted for SiO_2He at 610 GPa. Orange, blue, and red spheres represent He, Si, and O atoms, respectively. (b) Calculated phonon dispersions of SiO_2He at 610 GPa.

Surprisingly, He atoms are also surrounded by seven O atoms and two Si atoms with He-O distances ranging from 1.51 to 1.71 Å, resulting in HeO_7Si_2 polyhedra, which are similar to the SiO_7He_2 polyhedra (Fig. S1 in the SM). The volumes are 8.77 and 8.55 $Å^3$ for SiO_7He_2 and HeO_7Si_2 polyhedra at 610 GPa, respectively. Phonon calculations reveal no imaginary dispersions of SiO_2He at 610 [Fig. 2(b)], confirming the robust dynamic stability of SiO_2He. If we regard the SiO_2He phase as a prototype structure and replace all the He atoms with Si atoms, we then obtain a different SiO compound with the same *Pnma* symmetry which has a formation enthalpy of about −0.76 eV/atom (0.71 eV/atom) with respect to elemental Si and O (SiO_2 and Si) at 700 GPa. This suggests that the designed structure might be a metastable Si-O phase. Experimental synthesis of this phase would achieve a different Si-O compound with unconventional silicon coordination under high pressure.

Projected electronic band structures and projected density of states (PDOS) show that the SiO_2He is an insulator, as shown in Fig. 3. It is obvious to find that DOS near the Fermi level is dominated mainly by O atoms, although with a non-negligible contribution from Si and He atoms. Some bands near the Fermi levels exhibit a signature of mixed character, therefore confirming Si-O, He-O, and Si-He hybridized states (for example, along the T-Z, and U-R directions), which indicate there are interactions between them. The absence of electron localization between the Si and He, Si and O, and He and O in two-dimensional ELF of SiO_2He (Fig. S2) excludes the possible covalent bonds, while the Bader charge analysis shows that each Si donates ∼3.39 electrons: 3.31 to two O atoms and 0.08 to one He atom. This indicates the strong ionic bonds in Si-O and weak ionic bonds in Si-He.

The stable pressure and temperature (P-T) regions of SiO_2He are determined by free-energy calculations at high temperatures using the quasiharmonic approximation based on the phonon dispersions at 700, 800, 900, and 1000 GPa. The effect of temperature on the formation energy of SiO_2He with respect to the decomposition products SiO_2 and He is then examined at selected pressures. For example, the formation energy at 700 GPa increases to zero when the temperature is increased to 4500 K, above which SiO_2He decomposes. A critical P-T boundary of stability is then obtained for SiO_2He [white line in Fig. 4(a)]. AIMD simulations at three P-T points on the critical boundary were undertaken to examine the existence of the predicted SiO_2He in the stable P-T region. Figure 4(b) shows the calculated mean-squared displacement

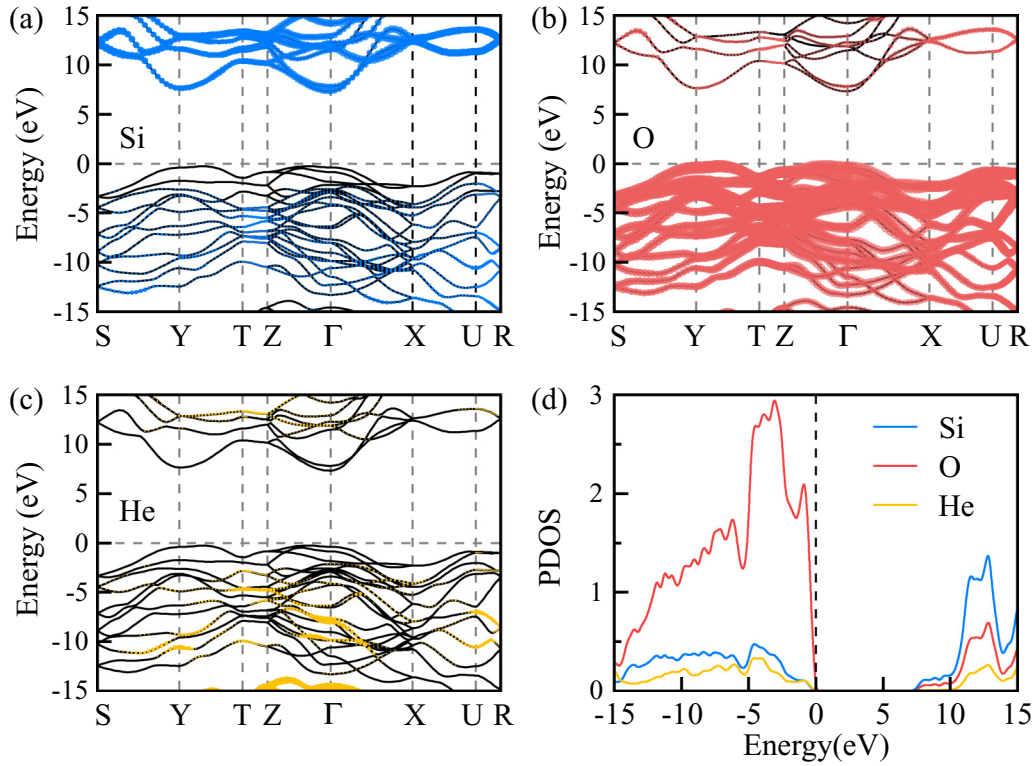

FIG. 3. The band structures of SiO_2He projected onto different atomic orbitals (a) Si, (b) O, and (c) He atoms, respectively, at 610 GPa. (d) Projected density of states (PDOS) of SiO_2He at 610 GPa.

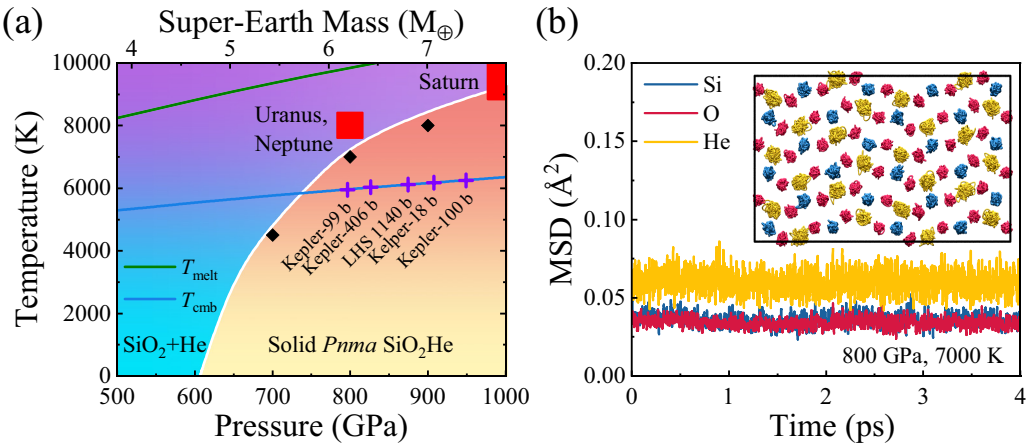

FIG. 4. (a) Pressure-temperature (P-T) phase diagram showing the stability field of SiO_2He and its boundary (white line) with the decomposition products SiO_2 + He. The proposed silica melting line ($T_m = 1968.5 + 307.8P_m^{0.485}$) [3] and the super-Earths' mantle adiabat [$T_{cmb} = 2275.2 + 1583.5(\frac{P}{129.8})^{0.485}$] [67] are plotted in green and blue, respectively. $P = 129.8(\frac{M_S}{M_E})$ links the pressure scale to the super-Earth mass (M_S) scale [67]. Red squares indicate the CMB of Uranus, Neptune, and Saturn [68]. Purple crosses indicate some Earth-like super-Earths with pressure corresponding to that in T_{cmb}, while the black rhombus represents the solid form of SiO_2He. (b) Calculated mean-squared displacement (MSD) of the atomic positions of SiO_2He at 800 GPa and 7000 K. The inset gives atomic trajectories in one supercell from the simulations in the last 2 ps. The blue, red, and orange colors represent the Si, O, and He atoms, respectively

(MSD) and trajectories of atoms at 800 GPa and 7000 K. All atoms in SiO_2He vibrate around their lattice positions with diffusion coefficients of zero, indicating a solid phase. Simulations at 700 GPa and 4500 K, and at 900 GPa and 8000 K (see Fig. S3 in the SM) give the same results, suggesting that SiO_2He remains solid over the entire stable P-T region. The solid SiO_2He at high temperature is different from the predicted diffused H in NH_3-He (at 2000 K and 100 GPa) and diffused He in H_2O-He (at 2000 K 100 GPa). This is understandable, considering the non-negligible interaction between the Si-He and O-He and the relatively large atomic masses of Si and O that trap He within cages formed by six surrounding SiO_7 motifs in SiO_2He.

The stable P-T region of SiO_2He covers the interior conditions of many planets (such as Saturn and super-Earths), indicating that SiO_2He might possibly constitute within planetary interiors if He could exist inside the planets. The yellow gradient area in Fig. 4(a) shows that stable solid SiO_2He could form inside gas giants and super-Earths. Figure S4 in the SM shows mass-radius relations for these Earth-like structures. Therefore, the prediction of SiO_2He could provide information for updating models of the interiors of planets (such as icy giant planets, Saturn, and super-Earths), and also provide important theoretical guidance for further examination of other He-containing minerals in planets, such as Al-O and S-O compounds.

IV. CONCLUSIONS

In conclusion, combining first-principles theory and structural prediction, we predict a SiO_2-He phase which is stable over a large pressure range from 607 GPa to at least 1 TPa at 0 K. It is composed of four equivalent SiO_7He_2 or HeO_7Si_2 polyhedra in the ground state of silicides. Both Si and He atoms in SiO_2He have a CN of nine: Each Si (He) atom is bonded with seven O atoms and two He (Si) atoms, forming Si-centered SiO_7He_2 (He-centered HeO_7Si_2) polyhedra. AIMD calculations show the possible existence of solid SiO_2He at the CMBs of the gas planets of our solar system as well as in super-Earths more massive than 5.7 $M_\oplus$. The present results not only benefit our understanding of the high-pressure behavior of materials, but can also broaden the family of He-containing compounds and provide guidance in updating the structural models and evolution of giant planets' interiors.

ACKNOWLEDGMENTS

The authors acknowledge funding from the NSFC under Grants No. 12074154, No. 12174160, No. 11804129, No. 11804128, and No. 11722433, and funding from the Science and Technology Project of Xuzhou under Grant No. KC19010. Y.L. acknowledges funding from the Six Talent Peaks Project and 333 High-level Talents Project of Jiangsu Province. All calculations were performed at the High Performance Computing Center of the School of Physics and Electronic Engineering of Jiangsu Normal University.

The authors declare no competing interests.

[1] K. Umemoto, R. M. Wentzcovitch, and P. B. Allen, Science **311**, 983 (2006).

[2] T. Tsuchiya and J. Tsuchiya, Proc. Natl. Acad. Sci. USA **108**, 1252 (2011).

[3] M. Millot, N. Dubrovinskaia, A. Černok, S. Blaha, L. Dubrovinsky, D. G. Braun, P. M. Celliers, G. W. Collins, J. H. Eggert, and R. Jeanloz, Science **347**, 418 (2015).

[4] L. Levien, C. T. Prewitt, and D. J. Weidner, Am. Mineral. **65**, 920 (1980).

[5] L. Levien and C. T. Prewitt, Am. Mineral. **66**, 324 (1981).

[6] N. L. Ross, J.-F. Shu, R. M. Hazen, and T. Gasparik, Am. Mineral. **75**, 739 (1990).

[7] M. Akaogi and A. Navrotsky, Phys. Earth Planet. Inter. **36**, 124 (1984).

[8] K. J. Kingma, R. E. Cohen, R. J. Hemley, and H.-K. Mao, Nature (London) **374**, 243 (1995).

[9] K. P. Driver, R. E. Cohen, Z. Wu, B. Militzer, P. L. Ríos, M. D. Towler, R. J. Needs, and J. W. Wilkins, Proc. Natl. Acad. Sci. USA **107**, 9519 (2010).

[10] L. S. Dubrovinsky, N. A. Dubrovinskaia, S. K. Saxena, F. Tutti, S. Rekhi, T. Le Bihan, G. Shen, and J. Hu, Chem. Phys. Lett. **333**, 264 (2001).

[11] A. R. Oganov, M. J. Gillan, and G. D. Price, Phys. Rev. B **71**, 064104 (2005).

[12] Y. Kuwayama, K. Hirose, N. Sata, and Y. Ohishi, Science **309**, 923 (2005).

[13] C. Prescher, V. B. Prakapenka, J. Stefanski, S. Jahn, L. B. Skinner, and Y. Wang, Proc. Natl. Acad. Sci. USA **114**, 10041 (2017).

[14] Y. Kono, Y. Shu, C. Kenney-Benson, Y. Wang, and G. Shen, Phys. Rev. Lett. **125**, 205701 (2020).

[15] C. Liu, J. Shi, H. Gao, J. Wang, Y. Han, X. Lu, H.-T. Wang, D. Xing, and J. Sun, Phys. Rev. Lett. **126**, 035701 (2021).

[16] M. J. Lyle, C. J. Pickard, and R. J. Needs, Proc. Natl. Acad. Sci. USA **112**, 6898 (2015).

[17] E. Bykova, M. Bykov, A. Černok, J. Tidholm, S. I. Simak, O. Hellman, M. P. Belov, I. A. Abrikosov, H.-P. Liermann, M. Hanfland *et al.*, Nat. Commun. **9**, 4789 (2018).

[18] T. Duffy, N. Madhusudhan, and K. Lee, in *Treatise on Geophysics*, edited by G. Schubert, Vol. 2 (Elsevier, Amsterdam, 2015).

[19] R. Scipioni, L. Stixrude, and M. P. Desjarlais, Proc. Natl. Acad. Sci. USA **114**, 9009 (2017).

[20] F. González-Cataldo, S. Davis, and G. Gutiérrez, Sci. Rep. **6**, 26537 (2016).

[21] H. Niu, A. R. Oganov, X.-Q. Chen, and D. Li, Sci. Rep. **5**, 18347 (2016).

[22] S. Wu, K. Umemoto, M. Ji, C.-Z. Wang, K.-M. Ho, and R. M. Wentzcovitch, Phys. Rev. B **83**, 184102 (2011).

[23] T. Guillot, Phys. Today **57**(4), 63 (2004).

[24] D. J. Stevenson, Proc. Natl. Acad. Sci. USA **105**, 11035 (2008).

[25] M. G. Jackson, J. G. Konter, and T. W. Becker, Nature (London) **542**, 340 (2017).

[26] J. Zhang, J. Lv, H. Li, X. Feng, C. Lu, S. A. T. Redfern, H. Liu, C. Chen, and Y. Ma, Phys. Rev. Lett. **121**, 255703 (2018).

[27] J. Zhang, H. Liu, Y. Ma, and C. Chen, Natl. Sci. Rev. (2021), doi: 10.1093/nsr/nwab168.

[28] N. Nettelmann, K. Wang, J. J. Fortney, S. Hamel, S. Yellamilli, M. Bethkenhagen, and R. Redmer, Icarus **275**, 107 (2016).

[29] C. Liu, H. Gao, Y. Wang, R. J. Needs, C. J. Pickard, J. Sun, H.-T. Wang, and D. Xing, Nat. Phys. **15**, 1065 (2019).

[30] H. Liu, Y. Yao, and D. D. Klug, Phys. Rev. B **91**, 014102 (2015).

[31] Y. Bai, Z. Liu, J. Botana, D. Yan, H.-Q. Lin, J. Sun, C. J. Pickard, R. J. Needs, and M.-S. Miao, Commun. Chem. **2**, 102 (2019).

[32] J. Shi, W. Cui, J. Hao, M. Xu, X. Wang, and Y. Li, Nat. Commun. **11**, 3164 (2020).

[33] C. Liu, H. Gao, A. Hermann, Y. Wang, M. Miao, C. J. Pickard, R. J. Needs, H.-T. Wang, D. Xing, and J. Sun, Phys. Rev. X **10**, 021007 (2020).

[34] H. Gao, C. Liu, A. Hermann, R. J. Needs, C. J. Pickard, H.-T. Wang, D. Xing, and J. Sun, Natl. Sci. Rev. **7**, 1540 (2020).

[35] B. Monserrat, M. Martinez-Canales, R. J. Needs, and C. J. Pickard, Phys. Rev. Lett. **121**, 015301 (2018).

[36] H. Gao, J. Sun, C. J. Pickard, and R. J. Needs, Phys. Rev. Materials **3**, 015002 (2019).

[37] Y. Li, X. Feng, H. Liu, J. Hao, S. A. T. Redfern, W. Lei, D. Liu, and Y. Ma, Nat. Commun. **9**, 722 (2018).

[38] X. Dong, A. R. Oganov, A. F. Goncharov, E. Stavrou, S. Lobanov, G. Saleh, G.-R. Qian, Q. Zhu, C. Gatti, V. L. Deringer *et al.*, Nat. Chem. **9**, 440 (2017).

[39] Z. Liu, J. Botana, A. Hermann, S. Valdez, E. Zurek, D. Yan, H.-Q. Lin, and M.-S. Miao, Nat. Commun. **9**, 951 (2018).

[40] Y. Wang, J. Zhang, H. Liu, and G. Yang, Chem. Phys. Lett. **640**, 115 (2015).

[41] S. Ding, J. Shi, J. Xie, W. Cui, P. Zhang, K. Yang, J. Hao, L. Zhang, and Y. Li, npj Comput. Mater. **7**, 89 (2021).

[42] T. Sato, H. Takada, T. Yagi, H. Gotou, T. Okada, D. Wakabayashi, and N. Funamori, Phys. Chem. Miner. **40**, 3 (2013).

[43] M. Matsui, T. Sato, and N. Funamori, Am. Mineral. **99**, 184 (2014).

[44] Y. Wang, J. Lv, L. Zhu, and Y. Ma, Phys. Rev. B **82**, 094116 (2010).

[45] Y. Wang, J. Lv, L. Zhu, and Y. Ma, Comput. Phys. Commun. **183**, 2063 (2012).

[46] B. Gao, P. Gao, S. Lu, J. Lv, Y. Wang, and Y. Ma, Sci. Bull. **64**, 301 (2019).

[47] M. Xu, C. Huang, Y. Li, S. Liu, X. Zhong, P. Jena, E. Kan, and Y. Wang, Phys. Rev. Lett. **124**, 067602 (2020).

[48] W. Cui and Y. Li, Chin. Phys. B **28**, 107104 (2019).

[49] B. Liu, W. Cui, J. Shi, L. Zhu, J. Chen, S. Lin, R. Su, J. Ma, K. Yang, M. Xu, J. Hao, A. P. Durajski, J. Qi, Y. Li, and Y. Li, Phys. Rev. B **98**, 174101 (2018).

[50] J. Chen, W. Cui, K. Gao, J. Hao, J. Shi, and Y. Li, Phys. Rev. Research **2**, 043435 (2020).

[51] W. Cui, T. Bi, J. Shi, Y. Li, H. Liu, E. Zurek, and R. J. Hemley, Phys. Rev. B **101**, 134504 (2020).

[52] K. Gao, W. Cui, J. Chen, Q. Wang, J. Hao, J. Shi, C. Liu, S. Botti, M. A. L. Marques, and Y. Li, Phys. Rev. B **104**, 214511 (2021).

[53] J. Ma, J. Kuang, W. Cui, J. Chen, K. Gao, J. Hao, J. Shi, and Y. Li, Chin. Phys. Lett. **38**, 027401 (2021).

[54] K. Gao, W. Cui, Q. Wang, J. Hao, J. Shi, S. Botti, M. A. L. Marques, and Y. Li, Phys. Rev. Materials **6**, 064801 (2022).

[55] J. Shi, W. Cui, S. Botti, and M. A. L. Marques, Phys. Rev. Materials **2**, 023604 (2018).

[56] P. Zhang, J. Shi, W. Cui, C. Liu, S. Ding, K. Yang, J. Hao, and Y. Li, Phys. Rev. B **105**, 214109 (2022).

[57] G. Kresse and J. Furthmüller, Phys. Rev. B **54**, 11169 (1996).

[58] G. Kresse and J. Furthmüller, Comput. Mater. Sci. **6**, 15 (1996).

[59] J. P. Perdew, J. A. Chevary, S. H. Vosko, K. A. Jackson, M. R. Pederson, D. J. Singh, and C. Fiolhais, Phys. Rev. B **46**, 6671 (1992).
[60] J. P. Perdew, K. Burke, and M. Ernzerhof, Phys. Rev. Lett. **77**, 3865 (1996).
[61] G. Kresse and D. Joubert, Phys. Rev. B **59**, 1758 (1999).
[62] A. Togo, F. Oba, and I. Tanaka, Phys. Rev. B **78**, 134106 (2008).
[63] S. Nosé, J. Chem. Phys. **81**, 511 (1984).
[64] W. G. Hoover, Phys. Rev. A **31**, 1695 (1985).
[65] K. Momma and F. Izumi, J. Appl. Crystallogr. **44**, 1272 (2011).
[66] See Supplemental Material at http://link.aps.org/supplemental/10.1103/PhysRevB.106.024102 for structural parameters, polyhedron structures, phonon dispersions, band gap at different pressures, MSD and atomic trajectories, and discovered super-Earths.
[67] F. W. Wagner, N. Tosi, F. Sohl, H. Rauer, and T. Spohn, Astron. Astrophys. **541**, A103 (2012).
[68] T. Guillot, Science **286**, 72 (1999).